Title

FLIm-Guided Raman Imaging to Study Cross-Linking and Calcification of Bovine Pericardium

Journal

Analytical Chemistry, 92(15)

ISSN

0003-2700

Authors

Shaik, Tanveer Ahmed
Alfonso-García, Alba
Zhou, Xiangnan
et al.

Publication Date

2020-08-04

DOI

10.1021/acs.analchem.0c01772

Peer reviewed

HHS Public Access

Author manuscript

Anal Chem. Author manuscript; available in PMC 2020 October 07.

Published in final edited form as:

Anal Chem. 2020 August 04; 92(15): 10659–10667. doi:10.1021/acs.analchem.0c01772.

FLIm-Guided Raman Imaging to Study Cross-Linking and Calcification of Bovine Pericardium

Tanveer Ahmed Shaik,
Leibniz Institute of Photonic Technology Jena e.V., 07745 Jena, Germany

Alba Alfonso-García,
Department of Biomedical Engineering, University of California Davis, Davis, California 95616, United States

Xiangnan Zhou,
Department of Biomedical Engineering, University of California Davis, Davis, California 95616, United States

Katherine M Arnold,
Department of Cardiovascular Diseases, Mayo Clinic, Rochester, Minnesota 55905, United States

Anne K Haudenschild,
Department of Biomedical Engineering, University of California Davis, Davis, California 95616, United States

Christoph Krafft,
Leibniz Institute of Photonic Technology Jena e.V., 07745 Jena, Germany

Leigh G Griffiths,
Department of Cardiovascular Diseases, Mayo Clinic, Rochester, Minnesota 55905, United States

Jürgen Popp,
Leibniz Institute of Photonic Technology Jena e.V., 07745 Jena, Germany; Institute of Physical Chemistry and Abbe Center of Photonics, Friedrich Schiller University Jena, 07743 Jena, Germany

Laura Marcu
Department of Biomedical Engineering, University of California Davis, Davis, California 95616, United States

Abstract

Bovine pericardium (BP) is a vascular biomaterial used in cardiovascular surgery that is typically cross-linked for masking antigenicity and enhance stability. There is a need for biochemical

Corresponding Authors: **Laura Marcu** – lmarcu@ucdavis.edu; **Jürgen Popp** – juergen.popp@ipht-jena.de.

Author Contributions

T.S. proposed the idea, methodology, performed data analysis, and wrote the manuscript, A.A.G. provided support on the methodology and valuable input in structuring and writing the manuscript, X.Z. provided support with FLIm acquisition code, K.A. performed HPLC measurements, A.K.H. provided inputs on methodology, C.K. provided input on Raman spectral data processing and manuscript preparation. A.A.G., X.Z., C.K., L.G., J.P., and L.M. participated in the layout and of the manuscript revision.

Complete contact information is available at: https://pubs.acs.org/10.1021/acs.analchem.0c01772

The authors declare no competing financial interest.

evaluation of the tissue properties prior to implantation to ensure that quality and reliability standards are met. Here, engineered antigen removed BP (ARBP) that was cross-linked with 0.2% and 0.6% glutaraldehyde (GA), and further calcified in vitro to simulate graft calcifications upon implantation was characterized nondestructively using fluorescence lifetime imaging (FLIm) to identify regions of interest which were then assessed by Raman spectroscopy. We observed that the tissue fluorescence lifetime shortened, and that Raman bands at 856, 935, 1282, and 1682 cm $^{-1}$ decreased, and at 1032 and 1627 cm^{-1} increased with increasing GA cross-linking. Independent classification analysis based on fluorescence lifetime and on Raman spectra discriminated between GA-ARBP and untreated ARBP with an accuracy of 91% and 66%, respectively. Pearson's correlation analysis showed a strong correlation between pyridinium cross-links measured with high-performance liquid chromatography and fluorescence lifetime measured at 380–400 nm (R = −0.76, p = 0.00094), as well as Raman bands at 856 cm^{-1} for hydroxy-proline (R = −0.68, p = 0.0056) and at 1032 cm^{-1} for hydroxy-pyridinium (R = 0.74, p = 0.0016). Calcified areas of GA cross-linked tissue showed characteristic hydroxyapatite (959 and 1038 cm^{-1}) bands in the Raman spectrum and fluorescence lifetime shortened by 0.4 ns compared to uncalcified regions. FLIm-guided Raman imaging could rapidly identify degrees of cross-linking and detected calcified regions with high chemical specificity, an ability that can be used to monitor tissue engineering processes for applications in regenerative medicine.

Graphical Abstract

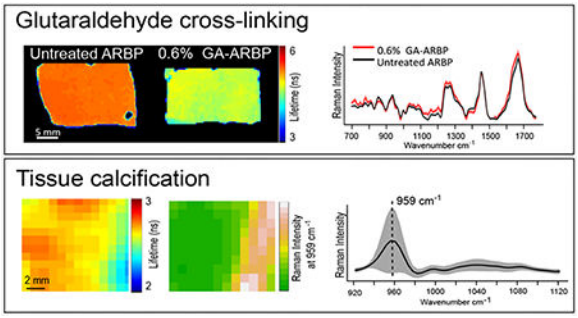

Vascular patches are clinically used to repair and reconstruct diseased tissue during cardiovascular surgeries.[1] Typically, such grafts are derived from synthetically engineered constructs, naturally occurring tissues from the patient (autologous grafts), or animal-derived substitutes (xenografts).[2] Bovine pericardium (BP) is widely used as a surgical material in cardiovascular clinical applications including manufacturing of vascular patches and heart valve bioprostheses.[3] The main component of BP is type I collagen (up to 90% dry weight).[4] Collagen is the most abundant structural protein in the extracellular matrix (ECM) in animals and humans.[5,6]

Typically, animal-derived tissues, such as BP, are preprocessed before implantation to mitigate adverse immune response from the host. To enhance biocompatibility, decellularization protocols or antigen removal (AR) processes are used to eliminate animal cell content and other adverse antigens.[1] Bioengineered grafts are further treated to enhance resistance against biodegradation and thrombogenesis. Glutaraldehyde (GA) is used as a chemical cross-linker that helps maintain the viscoelastic properties of the tissue while

preserving the native tissue architecture and enhancing the stability of collagen fibers in the ECM.[6,7] Cross-linking is particularly effective in BP due to the abundance of type I collagen in the biomaterial.[4] Cross-linking takes place through the reaction of an aldehyde group of GA with an amine group of lysine (Lys) or hydroxylysine (H-Lys) residues from the collagen molecules. This reaction results in the formation of Schiff bases further leading to the formation of GA-pyridinium type cross-links.[7,8]

It is established, however, that GA cross-linked tissues suffer from postimplantation calcification, which is a prominent reason for graft failure.[9] Calcification of heart valves mainly occurs because of the presence of free aldehydes in the GA molecules or residual antigenic components[4,10,11] that serve as nucleation sites for binding of extracellular calcium. This illustrates the importance of removing residual-free aldehydes prior to implantation.[12]

While excessive collagen cross-linking is detrimental for vascular graft applications, a weak ECM network leads to tissues that lack stability and integrity.[13] Hence, monitoring the correct degree of cross-linking and testing possible failure modes for each application is necessary. High-performance liquid chromatography (HPLC) is commonly used as gold standard to quantify collagen cross-links. However, this technique requires intense sample preparation, involves complex instrumentation, is time-consuming, and it requires destruction of the sample. These limitations hinder the translational ability of the technique for longitudinal monitoring and biochemical evaluation of bioengineered tissues in a nondestructive manner.

Label-free and nondestructive imaging techniques have the potential to address the needs of tissue engineering applications and provide quantitative biochemical assessment prior to tissue implantation. Fluorescence lifetime imaging (FLIm) and Raman spectroscopy require minimal sample preparation. In comparison to conventional quantification techniques such as HPLC or mechanical testing, the inherent nondestructive and label-free nature of FLIm and Raman spectroscopy can provide a spatially resolved and rapid assessment of tissue biochemical properties.[14–16] Thus, such approaches are better suited for longitudinal monitoring of tissue cross-linking processes and testing for subsequent causes of graft failure. Furthermore, FLIm and Raman spectroscopy can complement each other in assessing tissue biochemical information. FLIm can rapidly identify critical areas of biochemical contrast that can be used to selectively guide the acquisition of Raman spectra, which features enhanced biochemical specificity. Along with Raman spectroscopy, FLIm could be combined with other nondestructive and label-free optical modalities like optical coherence tomography (OCT),[17] intravascular ultrasound (IVUS)[18] and second harmonic generation (SHG/Multiphoton microscopy).[19,20] Complementary optical information can be obtained from each of these modalities.

Tissue fluorescence properties, and fluorescence lifetime in particular, are sensitive to changes in the collagen microenvironment of antigen removed bovine pericardium (ARBP).[21] In previous work, FLIm was used to detect collagen loss upon the digestion of BP with bacterial collagenase through the decrease in fluorescence lifetime, which correlated with the weakening mechanical properties of the tissue.[22] Raman imaging is inherently a slower

imaging technique than FLIm, but the spectral fingerprint provides molecular information on the composition of tissue, including secondary structural changes that occur in collagen.[13] In particular, changes in the proline, hydroxy-proline, C–C_α stretch, amide III and amide I regions and OH stretch[23] are all quantifiable using Raman imaging.[13,7]

The objectives of this study were to assess FLIm-guided Raman imaging as a nondestructive alternative to HPLC for monitoring the microenvironmental changes in ARBP upon GA cross-linking and to detect in vitro calcification in a label-free manner. The objectives were achieved by first investigating tissue fluorescence to identify regions of interest (ROIs). Those ROIs with altered fluorescence lifetime were then scanned for Raman spectral signatures of (1) ARBP cross-linked with increasing concentration of GA, and (2) calcified GA-ARBP mimicking possible causes of graft failure after implantation. Cross-linking was further quantified by HPLC and compared to the FLIm and Raman results through correlation analysis. Calcification deposits were further verified with ultrasound backscatter microscopy (UBM) imaging that provided cross-sectional images across thick tissue.

EXPERIMENTAL SECTION

Glutaraldehyde Cross-Linking of Bovine Pericardium.

Bovine pericardium (Spear Products, Coopersburg, PA) was subjected to antigen removal as previously described.[24] For cross-linking (Figure 1a), strips of ARBP were cut into 18 rectangular pieces of 2 cm × 1 cm. Samples were divided into three groups ($N = 6$ per group): cross-linked with 0.6% glutaraldehyde (GA; 25% Glutaraldehyde, Sigma-Aldrich) solution in PBS (0.6% GA group), cross-linked with 0.2% GA solution in PBS (0.2% GA group), and untreated ARBP kept in PBS. Concentrations lower than 0.2% aldehydes are ineffective sterilant against some mycobacteria, and higher than 0.6% aldehyde concentration results in excessive stiffing of tissue.[25,26] The samples were cross-linked on a shaker at 4 °C for 2 h. Following cross-linking, all samples were washed in PBS for 3 h. All sample preparations and wash buffer changes were done under sterile conditions.

Calcification of Cross-Linked Bovine Pericardium.

For in vitro calcification (Figure 1a), two strips (1 cm × 1 cm) of 0.6% GA cross-linked ARBP were used. One strip was calcified for three months in modified-simulated body fluid (m-SBF) solution[27] at 37 °C, and the other strip was used as a control, kept in PBS at 37 °C. Tissues were washed for 2 h prior to measuring with FLIm-guided Raman imaging and UBM.

FLIm Imaging System.

The FLIm system has been described previously.[28] Briefly, a frequency tripled Nd: YAG 355 nm laser (STV-02 × 10^{-1} × 0, TEEM Photonics, Grenoble, France; 1.2 μJ pulse energy, 4 kHz repetition rate) was used for FLIm excitation. The fluorescence signal was guided to a wavelength selection module (WSM) comprised of dichroic mirrors and bandpass filters that separate the autofluorescence (AF) in four spectral bands (SB) namely SB1 = 380–400 nm, SB2 = 415–455 nm, SB3 = 465–553 nm, SB4 = 572–642 nm. Only SB1, SB2, and SB3 were used in this study (as shown in Figure 1b) as they cover type I collagen emission upon

355 nm excitation. The AF signal from each spectral band was temporally separated using optical fiber delay lines of 1 m, 13 m, 25 m, and 37 m for each band, respectively. A single microchannel plate photomultiplier tube (MCP-PMT, R3809U-50, Hamamatsu, Japan) detected the AF signals that were further sampled at 12.5 GS/s by a high-speed digitizer (3 GHz bandwidth; PXIe–5185, National Instruments, Austin, Texas).

FLIm–Raman Multimodal Fiber Probe.

The FLIm-Raman probe used in this study was based on the design contained in U.S. patents 8,175,423 and 8,702,321.[29] Briefly, the probe consisted of a fiber bundle with 10 multimode fibers with 300 μm diameter core made of UV low–OH fluorine-doped fused silica (Figure 1c). The fibers were arranged such that the central fiber (in blue) was dedicated to FLIm excitation and collection with no additional filters at the distal end. One of the peripheral fibers (in red) delivered the Raman excitation laser at 785 nm. It contained a low-pass filter at the distal end to reduce the background. Raman collection was mediated through seven peripheral fibers (green), covered with a U-shaped high pass filter that rejected the laser line. All the fibers were tightly packed inside a stainless steel 14-gauge extra thin wall needle tube (1.82 mm i.d., 2.1 mm o.d.). A 0.2 NA lithium doped grin lens was mounted at the distal end of the fiber probe as an open tube attachment glued to the fiber bundle. This noncontact probe had a working distance of 1–1.5 mm. The fiber highlighted in gray was unused in this fiber bundle. The combined FLIm-Raman probe was mounted on a 3D translational stage (PROmech LP28, Parker, Charlotte, NC) used to raster scan the fiber across the sample creating 55 mm × 27 mm fluorescence lifetime maps with a step size of 250 μm × 250 μm (~14 min) and Raman acquisition took about at least 15 min to record 30 spectra.

Raman Spectroscopic System.

The seven Raman collection fibers were connected to a Raman spectrometer (LS-785, Princeton Instruments) equipped with an 830 grooves/mm reflective grating and a front-illuminated, open electrode CCD camera (PIXIS −256B, Princeton Instruments). The CCD was thermoelectrically cooled to −70 °C and the signal was collected with full range vertical binning. The Raman laser consists of a 785 nm multimode laser (0811A100-B model/Ocean optics, Innovative Photonics solutions) with excitation power fixed at 93 mW and Raman maps were recorded from regions of interest with 3 s exposure time and 10 accumulations per pixel. The spectral range was 200–3500 cm^{-1} with a spectral resolution of 15 cm^{-1}.

Ultrasound Backscatter Microscopy (UBM).

UBM data were acquired with a 4 mm aperture, 33 MHz ± 70% (fractional bandwidth) focused transducer (NIH UTRC, University of Southern California, Los Angeles, CA) that was positioned approximately 2 mm above the pericardium sample. An X-Y-Z translational stage was used for raster-scanning. A focused transducer was chosen to generate images with high-resolution and high SNR. Pulse generation and the collection was performed with a monocycle generator (AVB2-TE-C Avtech, Ogdensburg, NY), 30 dB amplifier, and an analog band-pass filter (10–100 MHz) before sampling at 400 MHz with a PCI digitizer (CS12400 Gage, Lockport, IL). For each location, 16 waveforms were averaged, leading to a spatial sampling of 250 μm in X and Y directions. For B-mode image reconstruction, signals

were processed by band-passed filtering from 20 to 60 MHz, envelope detection, and log-compression.

High-Performance Liquid Chromatography (HPLC).

Hydroxy-pyridinium cross-linking was quantified by HPLC. Tissue samples were first lyophilized and digested in 5 N HCl for 24 h, dried by speed vacuum evaporation, and subsequently resuspended in 0.12% heptafluorobutyric acid (HFBA) for analysis. Eight pyridinoline/deoxypryridinoline standards also suspended in 0.12% HFBA were run alongside samples for calibration. HPLC was performed using UltiMate 3000 Standard system (Thermo Fisher Scientific, Waltham, MA) and Syncronis C18 column (250 × 4.6 mm, 5 μm; Thermo Fisher Scientific, Waltham, MA) with all steps run at 40°C, at a flow rate of 1 mL/min. The mobile phase comprised of Solution A (0.12% HFBA in water) and Solution B (1:1 Acetonitrile to 0.12% HFBA). The column was equilibrated using 90% Solution A and 10% Solution B, elution utilized a linear gradient from 10% to 31% Solution B for 25 min followed by column washout with 75% Solution B and 25% Solution A for 15 min, and 15 min of re-equilibration. Pyridinoline fluorescence was detected using 295 nm excitation and 400 nm emission on a UVP fluorescent detector (Thermo Fisher Scientific Dionex Softron UltiMate 3000 detector, Waltham, MA).

Protocol for FLIm-Guided Raman Imaging.

First, the sample was scanned with FLIm. Fluorescence lifetime maps were displayed at the conclusion of the scan thanks to a LabVIEW tool that was developed based on the analog mean delay (AMD) technique.[30] Based on these near real-time fluorescence lifetime maps, regions of interest (ROI) 1.5 × 1.5 mm (36 FLIm pixels) were manually selected to guide the acquisition of Raman spectra (at least 30 Raman spectra) from every sample. Finally, the ROI was scanned for Raman imaging. All the tissues were kept hydrated with PBS during FLIm and Raman imaging.

FLIm Data Analysis.

Both spectrally resolved time-decay parameters and spectral ratios derived from the three spectral bands of the WSM were used in the analysis. To evaluate the fluorescence decay characteristics, the FLIm data was processed based on a constraint least-squares deconvolution with Laguerre basis functions as described previously.[31] Intensity ratios were calculated by dividing the fluorescence intensity of each spectral band by the sum of fluorescence intensities in all three spectral bands.[32] Data are presented as the mean and standard deviation from pixels within selected ROIs from all $N = 6$ samples per group. One-way ANOVA was performed to demonstrate the fluorescence lifetime contrast between the three distinct tissue groups in each spectral band. Linear discriminant analysis (LDA) was applied to fluorescence lifetime from three spectral bands with leave one out cross-validation (LOOCV).

Raman Spectra Preprocessing and Analysis.

Raman spectra were truncated from 700 to 1800 cm^{-1} for the analysis and the spectra were wavenumber and intensity calibrated. The fiber background was subtracted, and the

fluorescence baseline was corrected using Extended Multiplicative Signal Correction (EMSC), where four background component spectra and one/two pure components were used, the background components include an offset, two linear functions, and the fiber background. EMSC was implement using cbmodels package in R.[33] One pure component was the mean Raman spectrum of 0.6% GA-ARBP which was used for correcting 0.6% 0.2% GA-ARBP and untreated ARBP spectra. Two pure components were the mean Raman spectrum of 0.6% GA-ARBP and calcified GA-ARBP Raman spectrum which were used for correcting calcified spectra.

Raman spectra were smoothed using the function spc.loess (wavelength axis interpolation) from hyperSpec.[34] The 1452 cm^{-1} band was assigned to CH_2/CH_3 vibrations of collagen and elastin and the maximum was used for normalization as it has high SNR and is invariant to collagen structural changes upon GA cross-linking. All Raman spectra preprocessing was performed using hyperSpec[34] and cbmodels[33] packages in R. Partial least-squares–linear discriminant analysis (PLS-LDA) was performed on Raman data using the plslda and the cbmodels packages in R. The 26 spectra (700 cm^{-1} to 1770 cm^{-1}) with the highest SNR were selected for each sample for further analysis. PLS-LDA was performed on all groups together (0.6% GA-ARBP, 0.2% GA-ARBP, and untreated ARBP) and separately pairwise on 0.6% GA-ARBP versus untreated ARBP, 0.2% GA-ARBP versus untreated ARBP and 0.2% GA-ARBP versus 0.6% GA-ARBP. The PLS-LDA classifier performance of each model was evaluated with LOOCV, and the mean and standard deviation of the linear discriminant is shown.

RESULTS AND DISCUSSION

FLIm-Guided Raman Imaging to Detect GA Induced Cross-Links in Bovine Pericardium.

Representative fluorescence lifetime maps obtained for all three tissue groups investigated here (0.6% GA-ARBP, 0.2% GA-ARBP, and untreated ARBP) are depicted in Figure 2a–c. The FLIm maps showed distinct fluorescence lifetimes for different GA cross-linking concentrations. Fluorescence lifetime values ranged from 4.4 to 5.3 ns in SB1 and SB2, and from 3.9 to 4.7 ns in SB3. The fluorescence lifetime values in each of the SBs show a generalized decrease of lifetime with increasing GA concentration. One-way ANOVA comparing fluorescence lifetime values for each level of cross-linking concentration indicated that GA cross-linking significantly decreases the averaged lifetime of ARBP in each SB ($p < 0.001$) (Figure 2d–f). The type I collagen emission maximum is around 390 nm, attributed to the presence of hydroxy-pyridinium cross-links. Additional moieties in collagen also emit at 420–440 nm, however there is no evidence on the specific fluorophores in these bands.[35]

Unlike lifetimes, the intensity ratios do not significantly change upon cross-linking indicating that there are no spectral shifts and thus that the formation of intra- and intermolecular cross-links does not alter the overall content of the tissue.

A linear discriminant analysis (LDA) of the fluorescence lifetime data was done to further establish the classification ability of FLIm. An LDA model classified all three groups with an accuracy of 91%. Pairwise LDA models were also evaluated and showed that FLIm

differentiated between 0.2% GA-ARBP versus untreated ARBP with an accuracy of 100%, 0.6% GA-ARBP versus untreated ARBP with 100% accuracy, and 0.2% GA-ARBP versus 0.6% GA-ARBP with an accuracy of 84%. The corresponding sensitivities and specificities of each group for all the models are shown in Table 1. These classification results indicate that FLIm is able to identify the presence of cross-links induced by GA and to monitor the degree of cross-linking in the tissue. Cross-linking induces microenvironmental changes in the ECM of ARBP through intra- and intermolecular bonding between and within the collagen fibers, particularly hydroxy-pyridinium type cross-links.[36] These changes elicit lifetime contrast that can be further characterized through Raman spectroscopic analysis.

Using a similar FLIm setup, recent studies have shown that biochemical and biomechanical properties of different tissues are correlated with changes in fluorescence lifetimes.[6,22,37,32] In the present study, we show the fluorescence lifetime sensitivity to changes in the ECM matrix of ARBP induced by GA cross-linking. This could be used for quantitative and nondestructive monitoring of the degree of tissue cross-linking for quality control purposes during the tissue engineering process.

The fluorescence lifetime maps also served as a basis to acquire Raman spectra that provided enhanced specificity to the biochemical changes occurring in the tissue. Figure 3 shows the Raman spectral fingerprint region (700 cm^{-1} to 1770 cm^{-1}) of 0.6% GA-ARBP (a) and 0.2% GA-ARBP (b) compared to untreated ARBP. All the spectra from three groups confirmed that type I collagen is an abundant component of BP. The characteristic Raman bands observed in a type I collagen spectrum correspond to proline, hydroxy-proline, the C–C_α stretch in the α-helix conformation, amide III, and amide I (band assignments are compiled in Table 2). Collagen is a macromolecule composed of three polypeptide chains with an abundant amount of amino acid sequence repeats $(X\text{-}Y\text{-glycine})_n$ where X is proline and Y is hydroxy-proline. The three polypeptide chains are structurally arranged in a right-handed triple helix scheme.[7] A single polypeptide chain contains the X-Y-glycine sequence mainly formed by an α-helix structure. Raman spectroscopy has been previously used to detect α-helix and β-sheet structural changes in collagen.[13]

All spectral features that are discussed in the following section are changes relative to the peak at 1452 cm^{-1} that was used for normalization, as described in the Experimental Section. Upon GA cross-linking we observed a decrease in intensity at the hydroxy-proline (856 cm^{-1}) band. This change can be attributed to alterations in the lysine and hydroxylysines residues of collagen involved in the GA cross-linking process. An increase in intensity was observed at 1032 cm^{-1}, consistent with GA reacting with primary amines on BP that lead to the formation of collagen hydroxy-pyridinium cross-links.[7] Increases in the Raman intensity of GA cross-linked pericardia were also detected at 1305 cm^{-1}, which could be related to the C–H bending of aldehyde prior to the ether-type bond formation in the process of cross-linking.[13] The changes observed in the C–C_α stretch band (935 cm^{-1}), the amide I and amide III bands, along with the changes in hydroxy-proline, were attributed to the structural rearrangements of collagen upon cross-linking.[7]

Chemometric analysis of the Raman spectra provided further insight into the changes occurring at the molecular level. Partial least-squares–linear discriminant analysis (PLS-

LDA) was applied to Raman spectra to classify untreated ARBP from the different cross-linked tissues. A PLS-LDA model considering all the groups had an overall accuracy of 66%. This model (00,02,06) shows a clear ability to classify between the untreated and the treated groups, but the performance decreases when comparing between the different degrees of cross-linking (see Table 1 for details). Figure 3c shows the PLS-LDA predictions and corresponding real classes. The observed misclassifications in the prediction of 0.6% GA-ARBP arise because Raman spectroscopy does not excel in differentiating between the two cross-linked groups (0.2% and 0.6%), while it can clearly identify a GA-cross-linked tissue from a non-cross-linked tissue. The inability to separate between the cross-linked groups is reflected in the performance of the model, with poor sensitivity for the 0.2% group and poor specificity for the 0.6% group.

Figure 3d shows the associated spectral linear discriminant 1 (LD1) that features changes at the hydroxy-proline (856 cm^{-1}) band, with a negative peak attributed to the decrease of free hydroxy-proline residues of collagen, as an increasing proportion of those residues become involved in the GA cross-linking process. There was also a negative peak for C–C_α stretch (935 cm^{-1}) that indicates changes occurring at the α-helical conformation of type I collagen. An increase of intensity at 1032 cm^{-1} was assigned to hydroxy-pyridinium cross-links, consistent with the mechanism of GA cross-linking formation (GA induces 3,4,5 hydroxy-pyridinium cross-links[7]). A decrease at 1282 cm^{-1} in the amide III region, an increase at 1627 cm^{-1} and decrease at 1690 cm^{-1} in the amide I region were attributed to the conformational changes of the collagen structure induced by GA cross-links. No change at 1452 cm^{-1} and a decrease at 1466 cm^{-1} confirm the assumption that the peak at 1452 cm^{-1}, the CH_2/CH_3 deformation vibration band, is invariant upon cross-linking. These changes observed in LD1 were difficult to resolve in the overlaid spectra (Figure 3a, b) and demonstrate the added value of PLS-LDA.

Pairwise PLS-LDA models were applied on 0.2% GA-ARBP versus untreated ARBP and 0.6% GA-ARBP versus untreated ARBP to determine the ability of Raman spectroscopy to classify between cross-linked and untreated ARBP. The PLS-LDA of 0.2% GA-ARBP versus untreated ARBP classified the two groups with an accuracy of 95%. PLS–LDA of 0.6% GA-ARBP versus untreated ARBP classified the two groups with an accuracy of 97%. These results reiterate the ability of Raman spectroscopy to clearly identify GA cross-linked tissue. A third pairwise PLS–LDA model with 0.2% GA-ARBP versus 0.6% GA-ARBP classified the two groups with an accuracy of 52%. This indicates the challenge to discriminate between different degrees of cross-linking, and hence monitoring the process, with Raman spectroscopy which is consistent with the reduced accuracy of 84% of FLIm data. The corresponding sensitivities and specificities of the individual groups for all the models are shown in Table 1.

Comparing the performance of the FLIm and Raman models (Table 1) we observe that FLIm models outperform in monitoring the degree of cross-linking. Even when considering all the groups combined, FLIm could detect cross-linking changes with an accuracy of 91%, higher than the Raman model (66%). However, this comparison should be considered with caution as the Raman data set was smaller and was collected from ROIs only. To improve the

comparison between the FLIm and Raman models, it would be ideal to collect more Raman spectra from a larger number of independent, and rather homogeneous, tissue samples.

While FLIm excelled at monitoring cross-linking, Raman spectroscopy provided enhanced biochemical specificity. Raman data indicated the molecular changes occurring upon cross-linking, hence complementing the FLIm results. In summary, the microenvironmental changes in the ECM of GA cross-linked ARBP that resulted in decreased fluorescence lifetime (according to the FLIm maps) were further described by the Raman spectral features that identified specific conformational changes in the secondary structure of the collagen network (hydroxy-proline, C–C_α stretch, amide III region and amide I region).

Correlation of FLIm and Raman Results with HPLC.

HPLC remains the gold standard method to quantify cross-links.[39,40] Hydroxy-pyridinium cross-links were quantified from three groups (N = 5 tissue pieces per group) using HPLC. Untreated ARBP showed hydroxy-pyridinium cross-links ranging between 3.5 and 12 ng/mg, for 0.2% GA-ARBP these ranged between 7 and 28 ng/mg, and for 0.6% GA-ARBP between 17 and 54 ng/mg. Although the values strongly vary and overlap, a clear trend emerges that cross-links increase as a function of GA concentration. The overlap in the HPLC results is also consistent with the poorer separation between 0.2% and 0.6% GA-ARBP samples obtained by FLIm and Raman, as evident in Figures 2f and 3c and Table 1 (models 02,06). The results were correlated to fluorescence lifetime values in SB1 and to the mean Raman intensity maximum of hydroxy-proline (856 cm^{-1}) and hydroxy-pyridinium (1032 cm^{-1}) (see Figure 4).

Pearson's correlation analysis indicated a negative correlation between hydroxy-pyridinium cross-links (as quantified by HPLC) and fluorescence SB1 lifetimes (r = −0.76, p = 0.00094) (Figure 4a). It has been reported that hydroxy-pyridinium cross-link/pyridinoline from collagen fluoresce at ~385 nm upon 355 nm excitation.[39,41,36] A decreased fluorescence lifetime in SB1 was observed with increased GA cross-linking which could be related to the formation of GA induced hydroxy-pyridinium intra- and intermolecular cross-links in the pericardium ECM. This hypothesis is supported by the increase in the pyridinium cross-links measured with HPLC.

Pearson's correlation analysis was also performed on hydroxy-pyridinium cross-links (quantified using HPLC) and the Raman spectral bands corresponding to hydroxy-proline and hydroxy-pyridinium. Hydroxy-pyridinium cross-link and hydroxy-proline (856 cm^{-1}) were negatively correlated (r = −0.68, p = 0.0056) (Figure 4b). During cross-linking the lysine or hydroxy-lysine residues of collagen react with aldehyde groups (in our case GA) and intermediate reactions lead to the formation of hydroxy-pyridinium cross-link.[8] A negative correlation indicates a decrease in free hydroxy-proline residues of collagen, as an increasingly greater proportion of those residues become involved in the formation of cross-links. Conversely, a positive correlation was found between hydroxy-pyridinium cross-links (HPLC) and the hydroxy-pyridinium Raman band (r = 0.74, p = 0.0016) (Figure 4c), consistent with known mechanisms of action of GA that form 3,4,5 hydroxy-pyridinium cross-links.[7,8] The negative and positive correlations agree with negative spectral features at

856 cm^{-1} and positive spectral features at 1032 cm^{-1}, respectively, in Figure 3 upon GA cross-linking.

FLIm Guided Raman Imaging to Detect Calcification in Cross-Linked Bovine Pericardium.

Calcification is widely reported as a cause of failure of vascular grafts postimplantation. The ability to test for possible calcification events on the engineered tissues would provide FLIm-guided Raman additional benefits as a nondestructive tool for evaluating the performance of tissue engineered constructs. Extracellular calcium can alter the structural properties of GA-ARBP cross-links of the tissue, eliciting changes in the fluorescence lifetime.

Calcified GA-ARBP showed areas with shorter lifetime on the fluorescence map at SB1 (Figure 5a) that were used to guide acquisition of Raman spectra. These shorter lifetime areas (2.32 ± 0.09 ns versus 2.81 ± 0.07 ns in the PBS stored controls) showed a prominent hydroxyapatite (HA) bands at 959 cm^{-1} and a smaller one at 1038 cm^{-1} (Figure 5e). These are characteristic Raman bands associated with calcification that arise from symmetric and asymmetric stretching vibrations of PO_4^{3-}.[42,43] Of note, fluorescence lifetime in SB2 and SB3 also differed in calcified regions, but the mean lifetime difference was higher in SB1 (−0.49 ns) than in either SB2 (−0.2 ns) or SB3 (+0.2 ns).

Figure 5b and c show the transition area from longer to shorter lifetime (fluorescence lifetime map in SB1) and the Raman map obtained plotting the intensity at 959 cm^{-1}, respectively. This links the area of lower fluorescence lifetime in SB1 with calcified GA-ARBP.

Ultrasound backscattering microscopy (UBM) further verified the presence of the calcified area. Figure 5d shows a cross-sectional image of the corresponding calcified bovine pericardium piece. The white arrows point toward the calcified region of the tissue that appears much brighter and thinner than the rest of the tissue because the signal does not penetrate through calcification deposits.

CONCLUSION

The current study demonstrates an imaging strategy combining FLIm and Raman spectroscopy for nondestructive, in situ biochemical evaluation and testing of engineered vascular grafts. Specifically, we showed the ability of this approach to assess (1) collagen cross-linking and (2) calcification in vascular grafts. In this approach, areas of interest identified by FLIm were subsequently investigated by Raman spectroscopy, which besides providing detailed biochemical information can be used as an additional validation method for FLIm. Such strategy provides a path for biochemical evaluation and testing of engineered vascular grafts with high speed and biochemical specificity.

Fiber based FLIm-guided Raman spectroscopy was capable of monitoring and detecting GA cross-linking of ARBP by a specific Raman signature: decreased bands at 856, 935, 1282, and 1682 cm^{-1} and increased bands at 1032 and 1627 cm^{-1}. The fluorescence lifetime and the Raman signature could be used as an alternative tool to HPLC to quantify cross-links in

a nondestructive manner. The demonstrated ability of FLIm-guided Raman to detect calcified regions is useful for testing possible failure mechanisms in the developed grafts.

In conclusion, FLIm and Raman imaging has a strong potential to address some of the pressing needs for nondestructive and label-free monitoring of tissue engineering processes and their applications in regenerative medicine. The multimodal approach helps to probe additional biochemical and structural information, which improves the detailed characterization of tissues. In addition, the implementation of the technique mediated by an optical fiber probe has the potential to become a tool for assessing intraluminal graft performance in vitro and in vivo.

ACKNOWLEDGMENTS

We thank National Institutes of Health (NIH) (RO1HL1210689) and Jena-Davis Alliance of Excellence in Biophotonics (JEDIS) for the supporting the research work.

REFERENCES

(1). Pashneh-Tala S; MacNeil S; Claeyssens F Tissue Eng., Part B 2016, 22 (1), 68–100.

(2). Carrabba M; Madeddu P Front. Bioeng. Biotechnol 2018, 6 (4), 1–12. [PubMed: 29404323]

(3). Li X; Guo Y; Ziegler KR; Model LS; Eghbalieh SDD; Brenes RA; Kim ST; Shu C; Dardik A Ann. Vasc. Surg 2011, 25 (4), 561–568. [PubMed: 21276709]

(4). Schoen FJ; Tsao JW; Levy RJ Am. J. Pathol 1986, 123 (81760), 134–145. [PubMed: 2421577]

(5). Lodish H; Berk AZS Mol. Cell. Biol 5th ed; 2000 DOI: 10.1016/S1470-8175(01)00023-6.

(6). Sherlock BE; Harvestine JN; Mitra D; Haudenschild A; Hu J; Athanasiou KA; Leach JK; Marcu LJBiomed. Opt 2018, 23 (03), 1.

(7). Jastrzebska M; Wrzalik R; Kocot A; Zalewska-Rejdak J; Cwalina BJ Biomater. Sci., Polym. Ed 2003, 14 (2), 185–197.

(8). Olde Damink LHH; Dijkstra PJ; Van Luyn MJA; Van Wachem PB; Nieuwenhuis P; Feijen JJ Mater. Sci.: Mater. Med 1995, 6 (8), 460–472.

(9). Lee C; Kim SH; Choi SH; Kim YJ Eur. J. Cardio-thoracic Surg 2011, 39 (3), 381–387.

(10). Jorge-Herrero E; García Páez JM; Del Castillo-Olivares Ramos JL J. Appl. Biomater. Biomech 2005, 3 (2), 67–82. [PubMed: 20799226]

(11). Lim HG; Kim GB; Jeong S; Kim YJ Eur. J. Cardio-thoracic Surg 2015, 48 (1), 104–113.

(12). Saporito WF; Pires AC; Cardoso SH; Correa JA; Abreu LC; De; Valenti VE; Miller L; Colombari E BMC Surg. 2011, 11 (1), 37. [PubMed: 22192162]

(13). Martinez MG; Bullock AJ; MacNeil S; Rehman IU Appl. Spectrosc. Rev 2019, 54 (6), 509–542.

(14). Phipps JE; Gorpas D; Unger J; Darrow M; Bold RJ; Marcu L Automated Detection of Breast Cancer in Resected Specimens with Fluorescence Lifetime Imaging. Phys. Med. Biol 2018, 63 (1). 015003.

(15). Shipp DW; Rakha EA; Koloydenko AA; Macmillan RD; Ellis IO; Notingher I Breast Cancer Res. 2018, 20 (1), 69. [PubMed: 29986750]

(16). Manickavasagam A; Hirvonen LM; Melita LN; Chong EZ; Cook RJ; Bozec L; Festy F Analyst 2014, 139 (23), 6135–6143. [PubMed: 25318007]

(17). Kang WJ; Lee MW; Song JW; Kim JW; Oh W-Y; Nam HS; Yoo H Biomed. Opt. Express 2018, 9 (4), 1930. [PubMed: 29675330]

(18). Bec J; Phipps JE; Gorpas D; Ma D; Fatakdawala H; Margulies KB; Southard JA; Marcu L Sci. Rep 2017, 7 (1), 1–9. [PubMed: 28127051]

(19). Cicchi R; Baria E; Matthaus C; Lange M; Lattermann A; Brehm BR; Popp J; Pavone FS Characterization of Atherosclerotic Arterial Tissue Using Combined SHG and FLIM Microscopy In Advanced Microscopy Techniques IV; and Neuro-photonics II; Beaurepaire So P, Pavone F,

Hillman EE, Ed.; SPIE Proceedings; Optical Society of America: Munich, 2015; Vol. 9536, p 95360N DOI: 10.1364/ECBO.2015.95360N.

(20). Provenzano PP; Eliceiri KW; Keely PJ Clin. Exp. Metastasis 2009, 26 (4), 357–370. [PubMed: 18766302]

(21). Mitra D; Fatakdawala H; Nguyen-Truong M; Creecy A; Nyman J; Marcu L; Leach JK ACS Biomater. Sci. Eng 2017, 3 (9), 1944–1954. [PubMed: 28944287]

(22). Li C; Shklover J; Parvizi M; Sherlock BE; Alfonso Garcia A; Haudenschild AK; Griffiths LG; Marcu L Ann. Biomed. Eng 2018, 46 (11), 1870–1881. [PubMed: 30003502]

(23). Jastrzebska M; Wrzalik R; Kocot A; Zalewska-Rejdak J; Cwalina BJ Raman Spectrosc. 2003, 34 (6), 424–431.

(24). Wong ML; Wong JL; Athanasiou KA; Griffiths LG Acta Biomater. 2013, 9 (5), 6492–6501. [PubMed: 23321301]

(25). Jayakrishnan A; Jameela SR Biomaterials 1996, 17 (5), 471–484. [PubMed: 8991478]

(26). Griffiths G; Burke B; Lucocq J Fine Structure Immunocytochemistry; Springer-Verlag: Berlin; New York, 1993.

(27). Chen X; Li Y; Hodgson PD; Wen C Mater. Sci. Eng., C 2009, 29 (1), 165–171.

(28). Yankelevich DR; Ma D; Liu J; Sun Y; Sun Y; Bec J; Elson DS; Marcu L Design and Evaluation of a Device for Fast Multispectral Time-Resolved Fluorescence Spectroscopy and Imaging. Rev. Sci. Instrum 2014, 85 (3). 034303. [PubMed: 24689603]

(29). Dochow S; Ma D; Latka I; Bocklitz T; Hartl B; Bec J; Fatakdawala H; Marple E; Urmey K; Wachsmann-Hogiu S; Schmitt M; Marcu L; Popp J Anal. Bioanal Chem 2015, 407 (27), 8291–8301. [PubMed: 26093843]

(30). Moon S; Won Y; Kim DY Opt. Express 2009, 17 (4), 2834. [PubMed: 19219188]

(31). Liu J; Sun Y; Qi J; Marcu L Phys. Med. Biol 2012, 57 (4), 843–865. [PubMed: 22290334]

(32). Alfonso-Garcia A; Haudenschild AK; Marcu L Biomed. Opt. Express 2018, 9 (9), 4064. [PubMed: 30615748]

(33). Beleites C cbmodels: Collection of ‘Combined’ Models: PCA-LDA, PLS-LDA, PLS-LR as Well as EMSC, R Package Version 0.5-20150729. 2015.

(34). Beleites C; Sergo V HyperSpec: A Package to Handle Hyperspectral Data Sets in R. 2018.

(35). Marcu L; Cohen D; Maarek JI; M, W. S. G. Characterization of Type I, II, III, IV, and V Collagens by Time-Resolved Laser-Induced Fluorescence Spectroscopy. Proc. SPIE 3911, Opt. Biopsy III No. 4 2000 DOI: 10.1117/12.382720.

(36). Marcu L; French PMW; Elson DS Fluorescence Lifetime Spectroscopy and Imaging: Principles and Applications in Biomedical Diagnostics, 2014th ed.; Laura, Marcu, Paul MW, French DSE, Ed.; CRC Press, 2014 DOI: 10.1201/b17018.

(37). Haudenschild AK; Sherlock BE; Zhou X; Hu JC; Leach JK; Marcu L; Athanasiou KA J. Tissue Eng. Regener. Med 2019, 13 (4), 637–648.

(38). Krafft C; Codrich D; Pelizzo G; Sergo VJ Biophotonics 2008, 1 (2), 154–169. [PubMed: 19343646]

(39). Eyre D Annu. Rev. Biochem 1984, 53 (1), 717–748. [PubMed: 6148038]

(40). James IT; Walne AJ; Perrett D Ann. Clin. Biochem 1996, 33 (5), 397–420. [PubMed: 8888973]

(41). Fite BZ; Decaris M; Sun Y; Sun Y; Lam A; Ho CKL; Leach JK; Marcu L Tissue Eng., Part C 2011, 17 (4), 495–504.

(42). Tarnowski CP; Stewart S; Holder K; Campbell-Clark L; Thoma RJ; Adams AK; Moore MA; Morris MD J. Biomed. Opt 2003, 8 (2), 179. [PubMed: 12683843]

(43). Rehman I. ur; Movasaghi Z; Rehman S Vibrational Spectroscopy for Tissue Analysis; 2012 DOI: 10.1201/b12949.

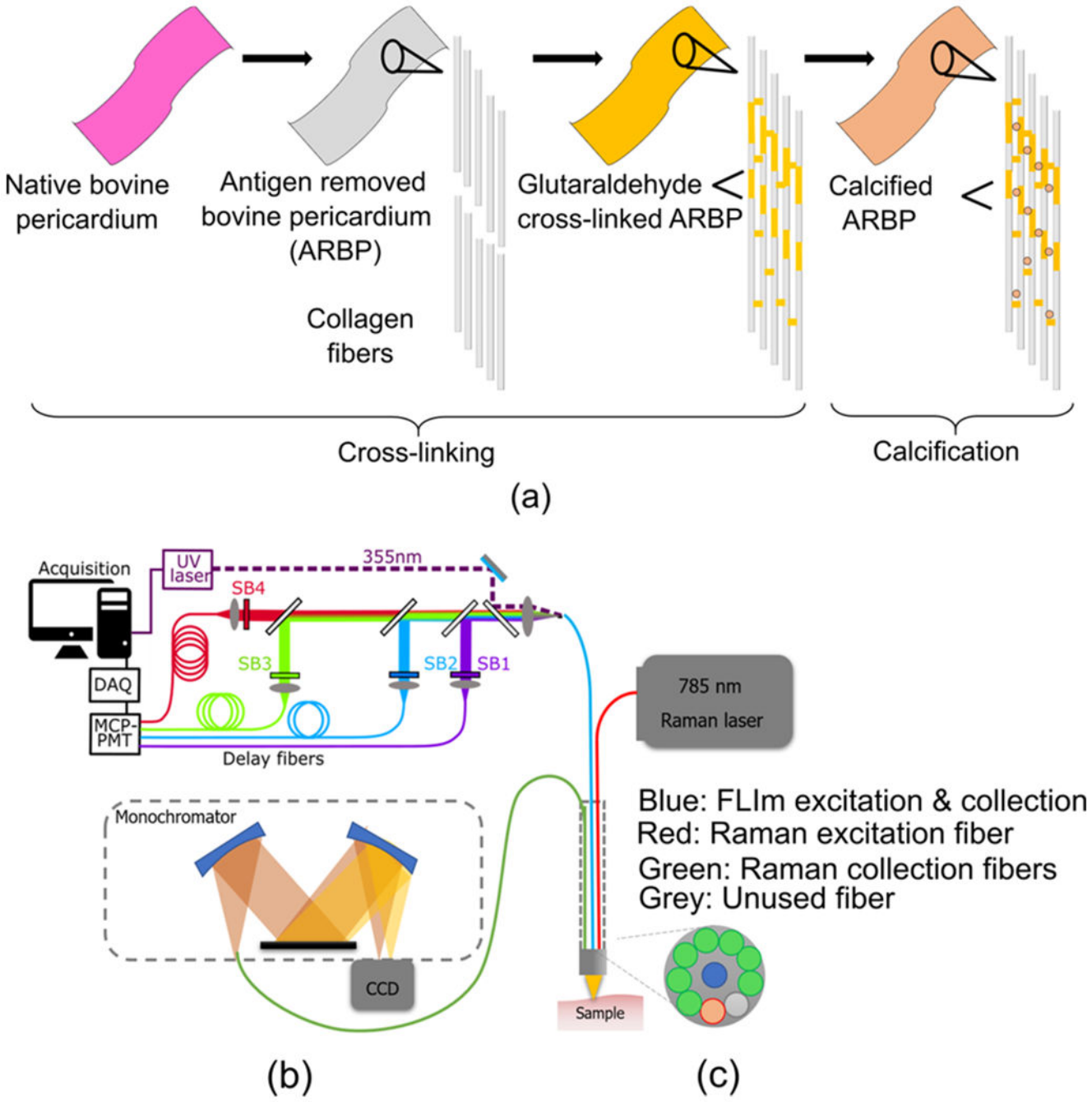

Figure 1.

(a) Experimental approach including glutaraldehyde cross-linking and calcification of antigen removed bovine pericardium (ARBP). (b) Schematic of the fiber-based FLIm-guided Raman imaging setup. (c) Combined FLIm – Raman fiber bundle probe.

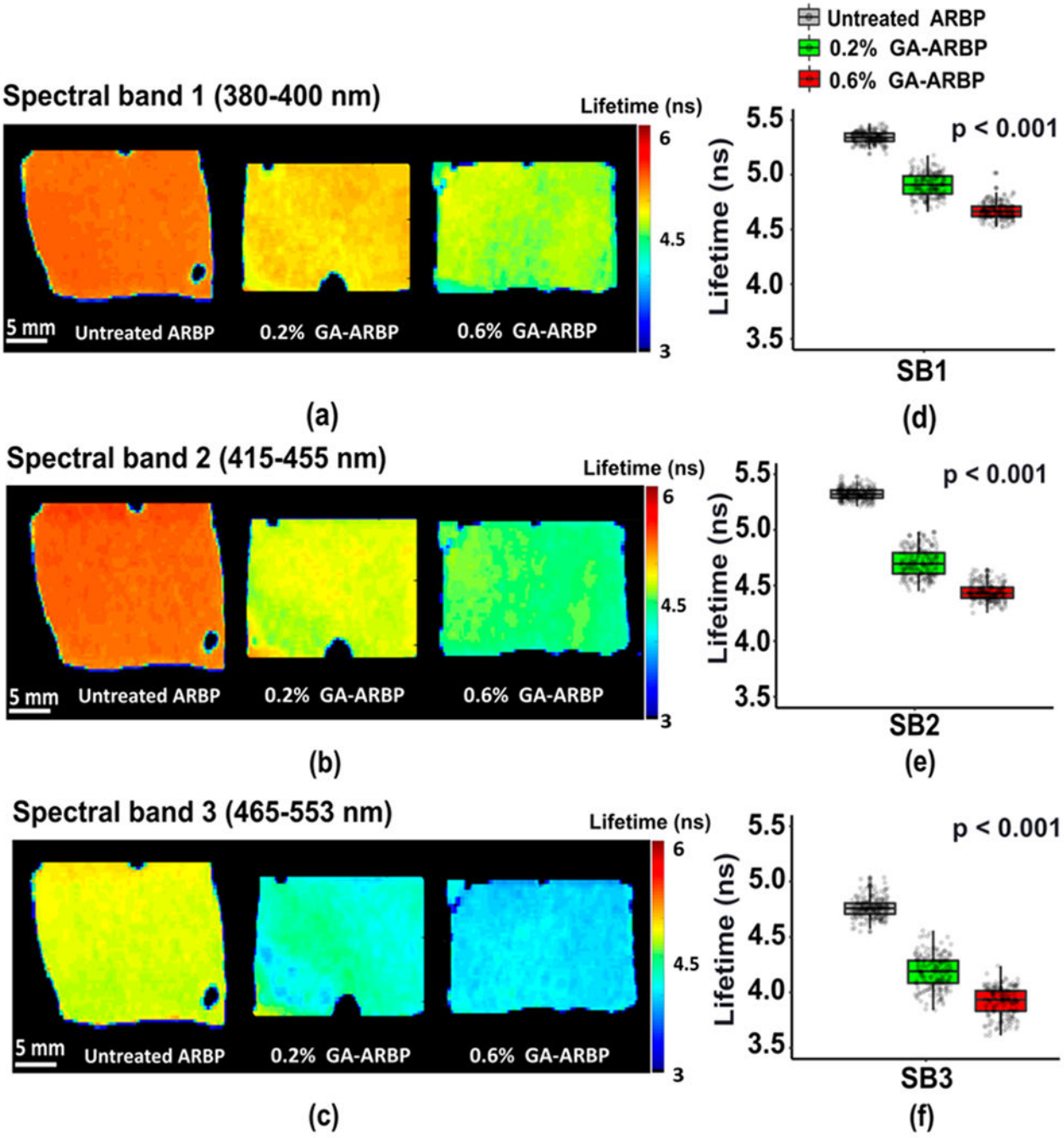

Figure 2.

Representative fluorescence lifetime maps of glutaraldehyde cross-linked antigen-removed bovine pericardium (GA-ARBP) and untreated antigen-removed bovine pericardium (untreated ARBP) in (a) SB 1, (b) SB 2, and (c) SB 3. The corresponding median and distribution of fluorescence lifetimes values for $N = 6$ in each tissue group for (d) SB 1, (e) SB 2, and (f) SB 3. One-way ANOVA indicated that all groups were significantly different from each other ($p < 0.001$).

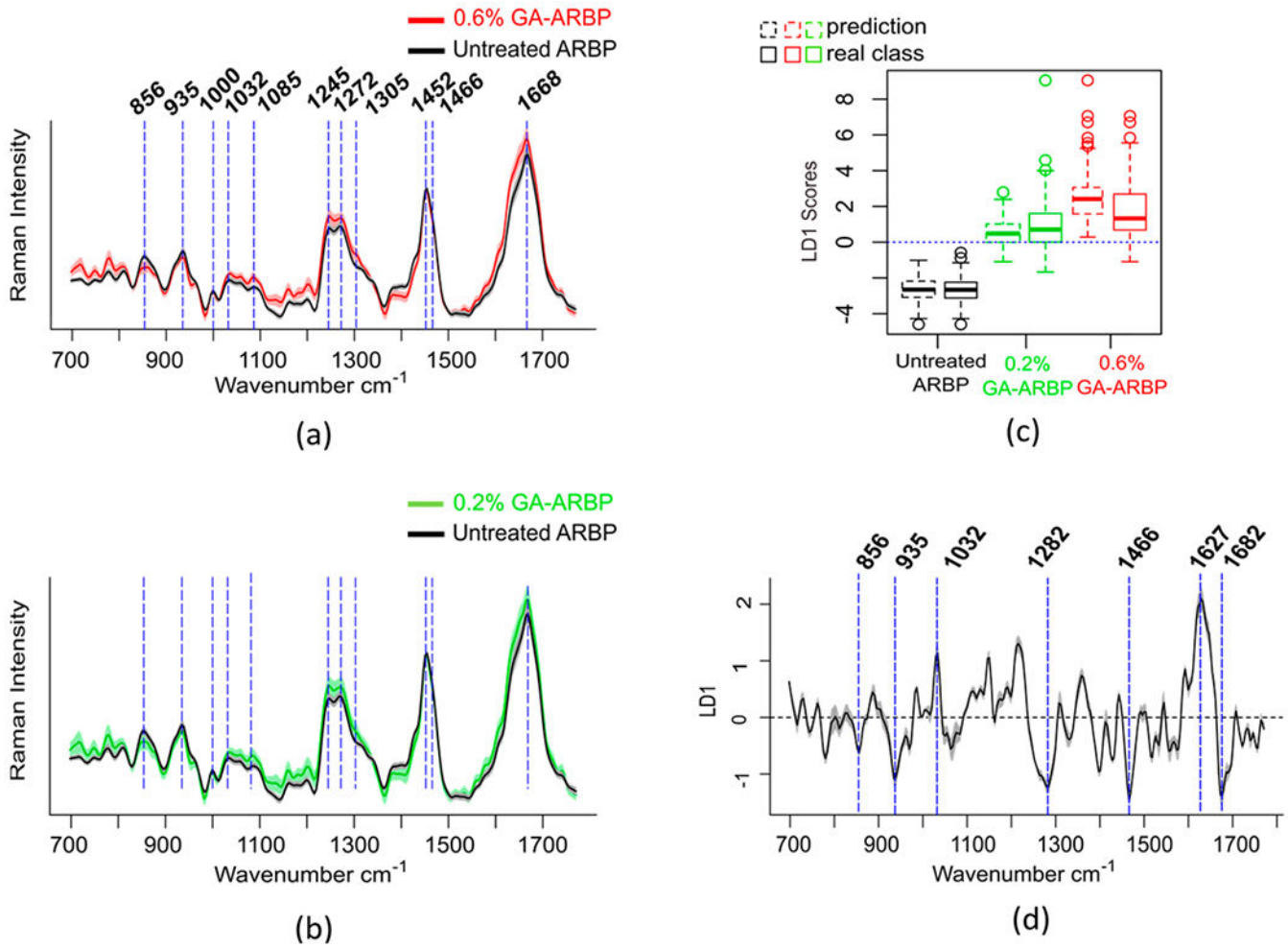

Figure 3.

Mean (thick line) and standard deviation (shaded area) of Raman spectra of untreated ARBP and 0.6% GA-ARBP (a), 0.2% GA-ARBP (b). Partial least-squares-linear discriminant analysis (PLS-LDA) of 0.6% GA-ARBP, 0.2% GA-ARBP and untreated ARBP, linear discriminant 1 (LD1) scores (c), and spectrum (d).

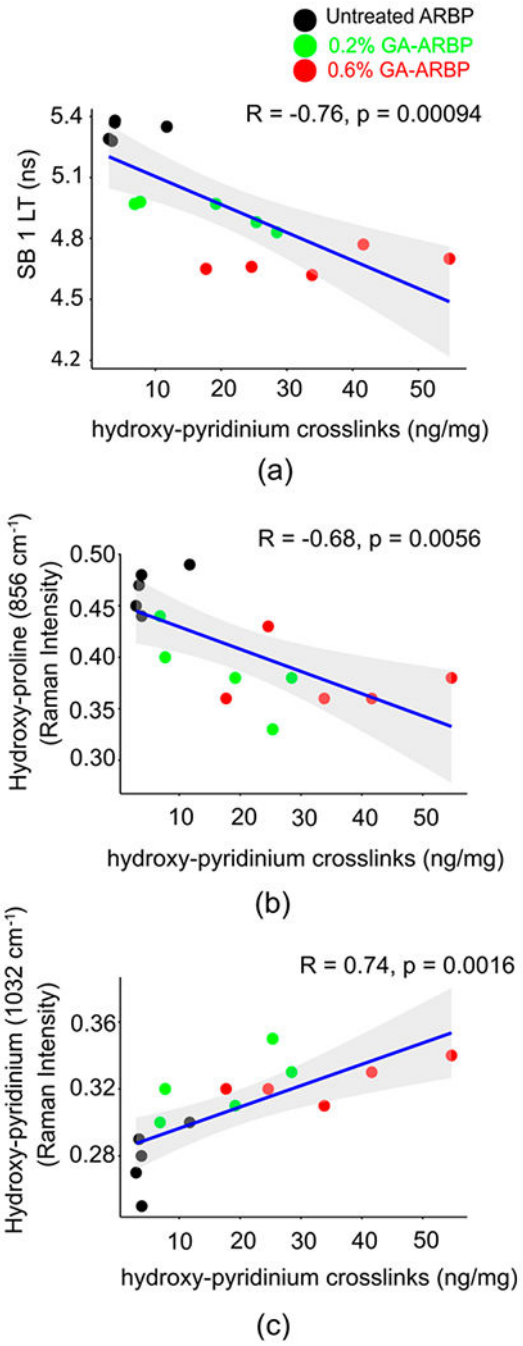

Figure 4.

FLIm and Raman spectra correlation with HPLC measurements of hydroxy-pyridinium cross-links. Pearson's correlation plots with (a) fluorescence lifetime in SB1, (b) hydroxy-proline Raman spectral band (856 cm^{-1}), and (c) hydroxy-pyridinium Raman spectral band (1032 cm^{-1}). The Pearson's correlation trend is shown with a thick line and the shaded region shows the confidence interval.

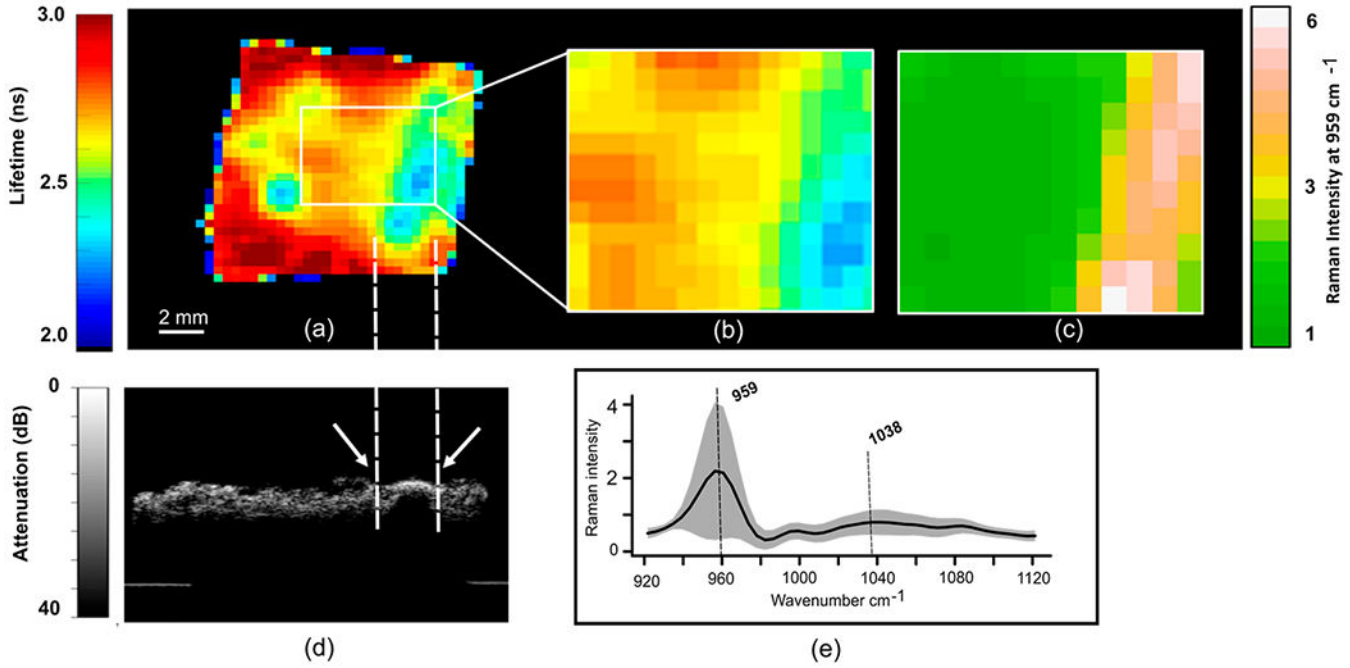

Figure 5.

FLIm guided Raman imaging to detect calcification. (a) Fluorescence lifetime map at spectral band 1 (390/18 nm) with highlighted ROI for Raman spectral acquisition. Zoomed ROI (b) FLIm in SB1, and (c) Raman intensity map using 959 cm^{-1} band. (d) Ultrasound image of tissue cross-section highlighting the calcified region (white arrows). (e) Raman spectral signatures of calcified GA-ARBP.

Table 1.

Accuracy (acc), Sensitivity (sen), and Specificity (spe) of Leave-One-Sample-out, Pixel-Level Classification of Untreated ARBP (00), 0.2% GA-ARBP (02), 0.6% GA-ARBP (06) Groups, Performed with FLIm and Raman Data

	model	Acc	sen00	spe00	sen02	spe02	sen06	spe06
FLIm	00,02,06	91	100	100	89	95	80	98
	00,02	100	100	100	100	100		
	00,06	100	100	100			100	100
	02,06	84			75	93	93	75
Raman	00,02,06	66	94	98	49	76	74	53
	00,02	95	99	91	91	99		
	00,06	97	100	94			94	100
	02,06	52			54	49	49	54

Table 2.

Raman band assignments for ARBP

wavenumber (cm^{-1})	band assignment
856	hydroxy-proline[38]
935	C–C_α stretch α – helix conformation triple helices[38]
1000	phenylalanine[7]
1032–35	hydroxy-pyridinium[7]
1085	C–O–C/ether[7]
1245	amide III[38]
1272	
1282	
1305	C–H bending[7]
1452	CH_2/CH_3 collagen and elastin[38]
1627	amide I[38]
1668	
1682	